



A mid-high spatial frequency error suppression method based on the pseudo-random path with space MABF mapping for complex surface

Wei Wang^{1,2} · Ruxin Gong¹ · Shijun Ji¹ · Ji Zhao^{1,3} · Xiaoya Li¹

Received: 4 September 2023 / Accepted: 29 November 2023 / Published online: 16 December 2023
© The Author(s), under exclusive licence to Springer-Verlag London Ltd., part of Springer Nature 2023

Abstract

Optical lenses, mirrors, and other precision optical components will inevitably produce errors in polishing. The errors in the mid-high spatial frequency (M-HSF) range will cause light scattering in different degrees and seriously affect the imaging performance of the optical system, such as contrast and reflectivity. The pseudo-random path has high direction randomness, effectively suppressing the machined surface's periodic polishing marks. In this study, a mesh surface pseudo-random path planning method based on the Matrix Angle-Based Flattening (MABF) algorithm is proposed to suppress the mid-high spatial frequency errors generated in the polishing process of free-form surface, and the application of the pseudo-random path planning method is extended from plane to complex surface. In order to improve the computational efficiency and reduce the deformation of the mesh in the parameterization process, an improved Angle-Based Flattening (ABF) algorithm called the MABF algorithm is proposed. Combined with MABF algorithm, a pseudo-random path planning method for complex surfaces is proposed based on space mapping. This method mainly includes pseudo-random path planning in the parameterized plane, path inverse mapping, and NURBS smoothing processing. The pseudo-random path obtained by this method has the advantages of smooth and uniform distribution. Simulation results show that the MABF algorithm is superior to the ABF algorithm in computing efficiency and error control. Simulations and experiments are conducted to verify the feasibility of the proposed path planning method in complex surface machining and the effectiveness of suppressing M-HSF errors.

Keywords Planar parameterization · Pseudo-random path · Free-form surface machining · Error suppression

Nomenclature

N_f	Total number of triangles in the mesh	d_l	Control points
f_i	The i th triangle in the mesh	ω_l	Weight factor
α_i^j	The angle at the j th vertex of the i th triangle in 2D mesh	K	The order of the polynomial curve
β_i^j	The angle at the j th vertex in the i th triangle in 3D mesh	U	Node vector
$N_{l,K}(u)$	Basis function	u_l	Elements of non-uniform and non-periodic node vector of U
		l_l	Nodes

✉ Shijun Ji
jishijun97@126.com

¹ School of Mechanical and Aerospace Engineering, Jilin University, Changchun 130025, Jilin, People's Republic of China

² School of Aeronautics and Astronautics, Sun Yat-sen University, Shenzhen 518107, Guangdong, People's Republic of China

³ School of Mechanical Engineering and Automation, Northeastern University, Shenyang 110819, Liaoning, People's Republic of China

1 Introduction

Precision optical components such as optical lenses and mirrors are essential in laser processing, national defense, and astronomical observation fields. The surface profile error and roughness of optical components play a decisive role in the whole equipment's performance. However, it is challenging to manufacture high-precision optical components. Precision optical components are usually polished to reduce microscopic surface irregularities. Tuell et al. believe that polishing will inevitably leave different spatial frequency

errors on the machined surface [1]. Generally, the low spatial frequency (LSF) error refers to the surface profile error, the middle spatial frequency (MSF) error refers to the surface waviness, and the high spatial frequency (HSF) error refers to the surface roughness. Different spatial frequency errors have different effects on the imaging results of the optical system. Achilles et al. found that M-HSF errors will scatter light and reduce contrast, which limits the performance of precision optical systems [2].

The machining path planning method for complex surfaces usually uses the iso-planar and iso-parametric methods [3]. Because of the single moving direction of the machining path, it is easy to generate periodic errors. Some studies have been carried out to suppress surface errors. Dong et al. analyzed the performance of three kinds of fractal fragmentation machining paths and proposed a random fractal-like path to better smooth surface texture and suppress surface ripples [4]. Nie et al. proposed a new polishing process based on magnetorheological finishing (MRF), smooth polishing, and ion beam figuring [5]. Smooth polishing is used to suppress MSF errors and MRF is used to suppress most of the LSF errors. Feng et al. proved that the polishing path obtained by the circular interpolation method can balance the contour error and power spectral density (PSD) curves [6]. Wan et al. proposed the use of a bi-step raster path to suppress the first two-order peaks of the error spectrum to reduce the MSF errors [7]. Hu et al. used a combination of MRF and smooth polishing to suppress surface errors [8]. MRF was used to suppress LSF errors, and smooth polishing based on a pseudo-random path was used to suppress M-HSF errors. Del Hoyo et al. investigated the relationship between processing parameters and PSD to suppress HSF errors by optimizing the processing parameters [9]. Lin et al. found that the use of flexible grinding wheels resulted in lower LSF errors and HSF errors than the use of rigid grinding wheels and could suppress some MSF errors during the grinding of optical fused silica [10]. Takizawa et al. used a pseudo-random path based on circular elements to suppress repetitive patterns on polished surfaces, and the surface ripple obtained using this path was significantly better than other pseudo-random paths [11]. Zha et al. used both changing the direction of path formation and the path spacing to avoid superposition of the convolution effect during polishing [12]. Huang et al. proposed a pseudo-random based on the traveling salesman problem to reduce the impact of periodic polishing paths [13]. The path divides the processing point into sections by clustering, then solves the optimal path for each subclass, and finally merges the subclasses. Maloney et al. concluded that MRF can be used to suppress LSF errors of optical components [14]. Dai et al. combined a part-random path based on maximum entropy theory with MRF to obtain a part with high shape accuracy and low MSF errors [15]. However, these studies mainly focus on the

polishing of flat or simple surfaces and do not applicable to complex surfaces.

This study focuses on the use of pseudo-random paths to suppress M-HSF errors generated in free-form surface polishing. The specific method is to use the pseudo-random path planning method of mesh surface based on the MABF algorithm to create smooth and uniformly distributed pseudo-random paths on the free-form surface, as is shown in Fig. 1. Section 2 describes the MABF algorithm and the planar parameterization, which transforms the path planning problem from the free-form surface into a plane. A pseudo-random path planning method for arbitrary boundary regions is presented in Section 3. In Section 4, the pseudo-random path on the plane is inversely mapped to free-form surface by the area coordinate method, and NURBS smoothing is applied to the path. In Section 5, five different pseudo-random path planning methods are compared and the superiority of the proposed path planning method in this study is demonstrated. Then the feasibility of the proposed path planning method is verified by simulation of some cases. Verification experiments on the effectiveness of the pseudo-random machining path based on space MABF mapping for suppressing M-HSF errors in free-form surface polishing are conducted in Section 6.

2 Planar parameterization using the MABF algorithm

2.1 MABF algorithm

Planar parameterization is a method of converting mesh surfaces to mesh planes, and it allows the features of each triangle to be preserved as much as possible during the conversion. For uniformity of machining paths on free-form surfaces, machining paths are planned based on the mesh parameterization method. The original free-form surface is divided into triangular meshes, and each triangle is mapped to the plane according to the position and geometric relationship. In this process, triangles are deformed to different degrees. The traditional Angle-Based Flattening (ABF) algorithm ensures that the angle change of each triangle before and after the planar parameterization is minimized and the geometric features of each triangle are retained to a maximum extent, thus reducing the deformation of the mesh during the mapping process. Traditional ABF algorithm uses the iterative solution method to obtain the optimal solution of large sparse matrices under constraints, which has high complexity, large computation, and low convergence efficiency. The MABF algorithm is proposed to improve computational efficiency and accuracy.

The basic principle of the MABF algorithm is to transform the planar parameterization problem into the

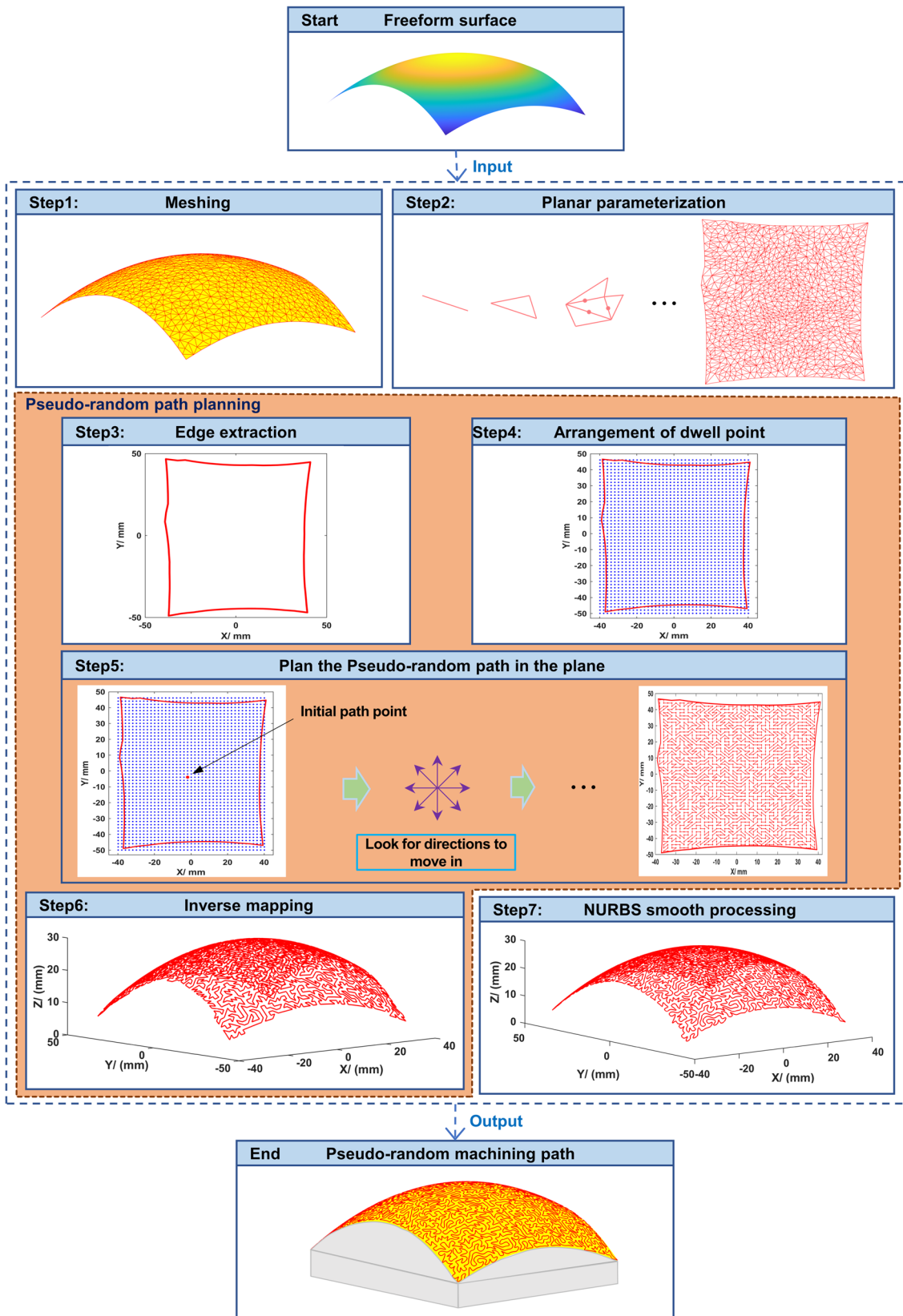


Fig. 1 The generation process of pseudo-random machining path based on space MABF mapping

computation of the optimal solution of the energy target equation for the mesh surface under constraints. When mapping a free-form surface from 3D to 2D using the MABF algorithm, each triangle needs to satisfy the following three conditions after parameterization:

1. The sum of the interior angles of each triangle is 180° .
2. The common sides of two adjacent triangles have the same length.
3. The sum of the angles connecting the inner vertices (non-boundary points) is 360° .

The above three constraints are expressed in matrix form as Eq. 1.

$$\begin{cases} A\vec{\alpha} - \pi = 0 \\ B\vec{\alpha} - 2\pi = 0 \\ C \ln(\sin \vec{\alpha}) = 0 \end{cases} \quad (1)$$

$$\vec{\alpha} = [\alpha_1^1, \alpha_1^2, \alpha_1^3, \alpha_2^1, \alpha_2^2, \alpha_2^3, \dots, \alpha_{N_f}^1, \alpha_{N_f}^2, \alpha_{N_f}^3]^T \quad (2)$$

$$A = \begin{bmatrix} 1 & 1 & 1 & & & & 0 & 0 & 0 \\ & & & 1 & 1 & 1 & & & \\ & & & & & & & & \\ & & & & & & & & \\ & & & & & & & & \\ & & & & & & & & \\ 0 & 0 & 0 & & & & 1 & 1 & 1 \end{bmatrix} \quad (3)$$

where $\vec{\alpha}$ is the angle of all triangles in the parameter plane. B and C are large sparse matrices. The number of rows is the number of internal vertices in the mesh and the number of columns is the number of angles in the mesh. For B , if the angle corresponding to the column number is connected to the vertex corresponding to the row number, the element in the matrix is 1. For C , the element whose row number is the vertex number and whose column number is the last number of the angle connected to the vertex is 1. The element whose row number is the vertex number and whose column number is the next number of the angle connected to the vertex is -1 .

The deformation energy equation in matrix form is Eq. 4.

$$E(\alpha) = \min \|I_{3 \times N_f} \times \vec{\alpha} - \vec{\beta}\|_F \quad (4)$$

where E is the deformation energy, and $\vec{\beta}$ is the angle of each grid in the original surface.

$$\vec{\beta} = [\beta_1^1, \beta_1^2, \beta_1^3, \beta_2^1, \beta_2^2, \beta_2^3, \dots, \beta_{N_f}^1, \beta_{N_f}^2, \beta_{N_f}^3] \quad (5)$$

The planar parameterization problem is transformed into an optimization problem under nonlinear constraints with large sparse matrices. In order to verify the effectiveness of the

MABF algorithm, three models of hemispherical, pentagonal, and saddle-shaped surfaces were simulated using the MABF algorithm and the ABF algorithm, respectively, in MATLAB R2021a and the computational time and errors were compared.

For the hemispherical surface, the program running time of the ABF algorithm was 351.89 s, and the calculation error is shown in Fig. 2a–b. Using the MABF algorithm, the program runs in 5.56 s and the calculation error is shown in Fig. 2c–d. The simulation results show that the computational efficiency of the MABF algorithm is significantly better than that of the ABF algorithm, and both algorithms get similar errors in the sum of the interior angles of triangles and the sum of peripheral angles of the vertices. The mesh deformation of the two algorithms will be compared in the next section. Regarding computation time consumed, the ABF algorithm is more sensitive to the number of triangles than the MABF algorithm. Table 1 shows the time the two algorithms consume to compute some mesh surfaces.

2.2 Planar parameterization

The MABF and the ABF algorithms use the free boundary method in the planar parameterization. Selecting a starting position of the planar parameterization near the center of the surface and then expanding it outward according to the mesh's geometry. The ABF algorithm first selects an initial edge near the center of the mesh surface to determine the two initial triangles and then expands in all directions based on the other edges of these two initial triangles. However, due to errors in the geometric parameters of the triangles obtained in Section 2.1, using this method will make the errors accumulate in the same direction in the process of planar parameterization. It can produce large deviations at points that should coincide, resulting in severe deformation of some mesh regions in the parameterized plane and increasing the risk of mesh overlap after planar parameterization. MABF algorithm assumes that the geometric parameters of triangles remain the same before and after parameterization, and selects the midpoints of the three sides of each triangle as the extension datum instead of the three edges. The initial triangle is selected near the center of the mesh surface, and the midpoints of the corresponding edges of the adjacent triangles coincide with the midpoints of the initial triangle. The direction of the adjacent triangles can be determined according to the direction of the edges of the initial triangle. At this point, the position and direction of the adjacent triangles can be determined. Repeat this process until all triangles on mesh surfaces have completed the planar parameterization process.

Each mesh vertex after parameterization takes the average of multiple points. The planar parameterization based on the MABF algorithm fully considers the error accumulation in the planar parameterization and disperses the error to the vertices of each triangle, which avoids the error accumulation effectively. The planar

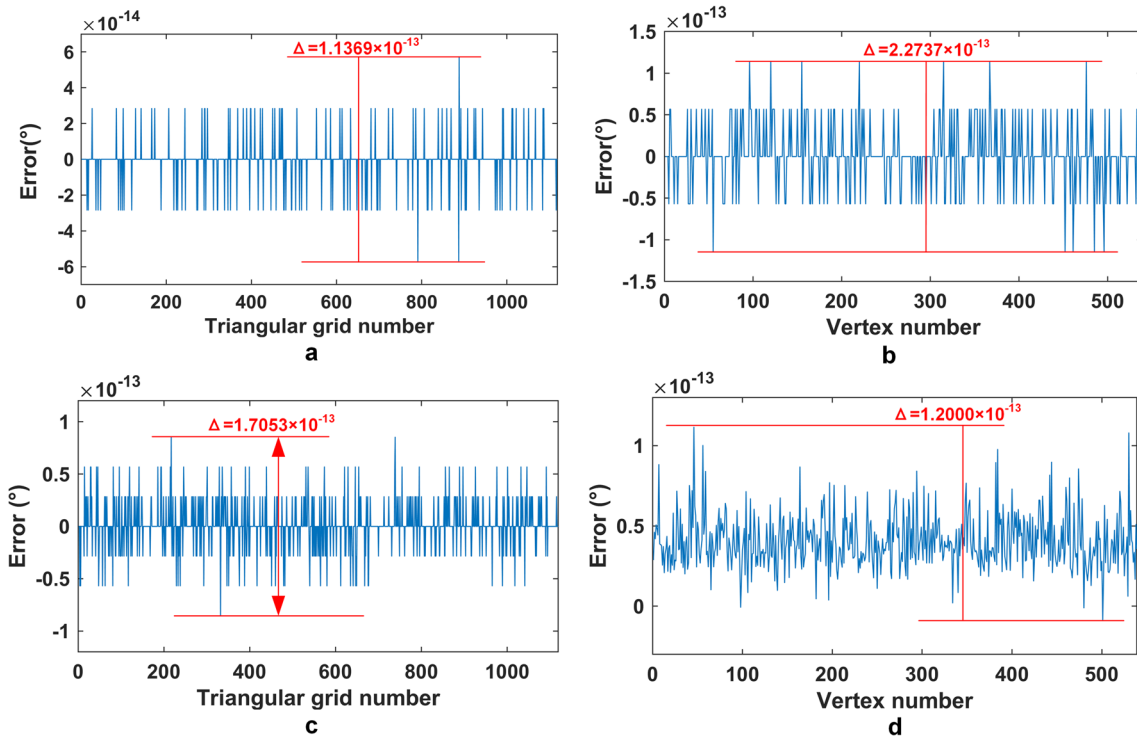


Fig. 2 **a** The errors in the sum of the interior angles of triangles obtained by ABF algorithm. **b** The errors in the sum of peripheral angles of the vertexes obtained by ABF algorithm. **c** The errors in the

sum of the interior angles of triangles obtained by MABF algorithm. **d** The errors in the sum of peripheral angles of the vertexes obtained by MABF algorithm

Table 1 Time-consuming comparison of ABF and MABF algorithms

Case	Mesh quantity	Algorithm	Time consuming (s)
Hemispherical surface	1119	ABF	351.89
		MABF	5.56
Five-pointed star	3559	ABF	1059.16
		MABF	69.33
Airfoil	4563	ABF	3456.26
		MABF	158.54
Saddle surface	5000	ABF	8432.58
		MABF	178.70

parameterization method based on the MABF algorithm can effectively reduce the mesh’s deformation in the planar parameterization process and improve the accuracy of parameterization and path inverse mapping. The results of planar parameterization of the two algorithms are shown in Fig. 3.

3 Pseudo-random path planning

Beaucamp et al. believe that the pseudo-random path can reduce the regular marks left by periodic machining paths on the surface and is used to suppress the MSF errors

generated by sub-aperture polishing tools on the workpiece surface [16]. In optical imaging, periodic slight marks will scatter light, reducing the optical system’s contrast and reflectivity. The pseudo-random path increases the randomness of the machining path. Each new path point is randomly selected from the unpassed points around the last dwell point of the current path. The initial path point has eight moveable directions. The pseudo-random paths have the following characteristics:

1. The machining path passes through all the set dwell points in the machining area.
2. Each dwell point is passed through only once.
3. The machining paths are continuous and do not cross.
4. The path has strong adaptability to the shape of the polishing area.

The planning process of the pseudo-random path is shown in Fig. 4.

1. Presetting the dwell points in the machining area and then randomly selecting a path point (Proximity to the center of the processing area is recommended) as the initial point of the path.

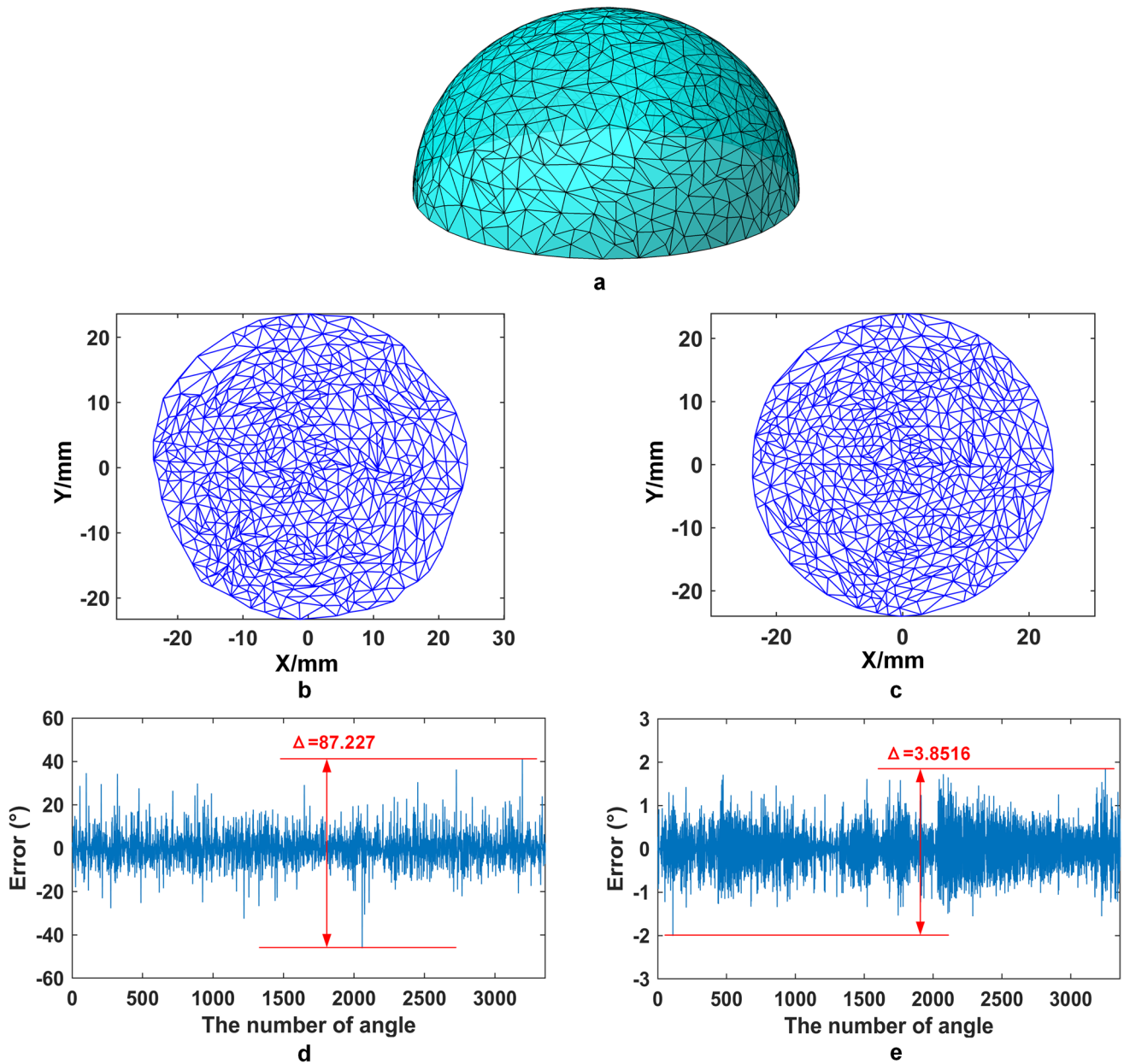


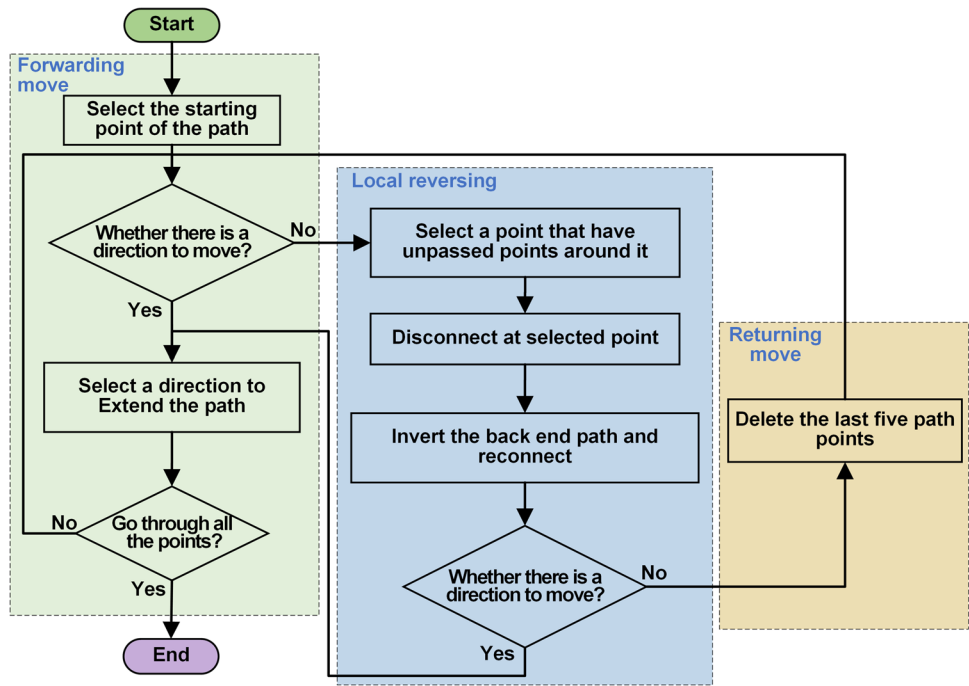
Fig. 3 Comparison of deformation degree of different planar parameterization methods. **a** Hemispherical surface. **b** The planar parameterization results of ABF algorithm. **c** The planar parameterization

results of MABF algorithm. **d** The angle errors of mesh obtained by ABF algorithm. **e** The angle errors of mesh obtained by MABF algorithm

2. Randomly select an unpassed dwell point around the current point as the next path point.
3. Repeat step 2 until all preset dwell points have been passed.
If the path enters the dead zone, that is, all surrounding dwell points have been passed and there is no alternative direction for the next path point, perform the local turnaround step (step 4–step 6).

4. Around the current path point, select a path point that exists an unpassed dwell point around it and disconnect at that point.
5. Reverse the order of the paths after the breakpoint location, and then reconnect the two paths in order.
6. Determines whether there are unpassed dwell points around the current path point. If so, return to step 2. If not, go to step 7.

Fig. 4 The process of the pseudo-random path planning method



7. Return to step 5 and delete the last five path points, then return to step 2.

A bicycle seat surface (as shown in Fig. 5a) is taken as the model, and the model was planar parameterized using the MABF algorithm. Then, the pseudo-random machining path is planned in the obtained plane, and the in-plane machining path is obtained, as shown in Fig. 5b.

4 Path inverse mapping

4.1 Path inverse mapping algorithm

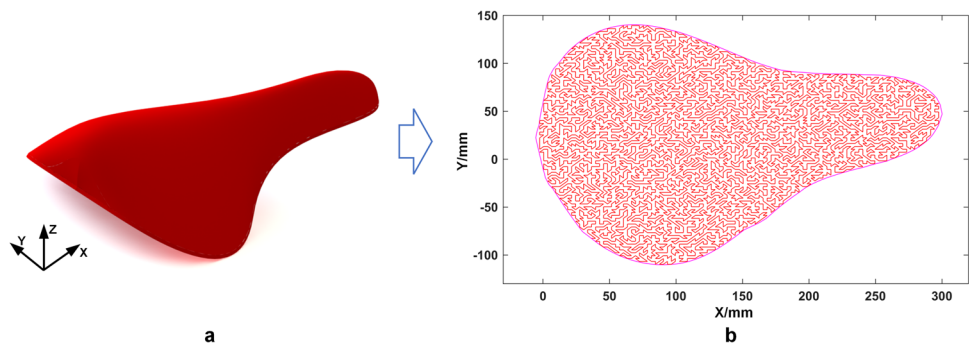
To achieve a uniform machining path on a free-form surface, it is necessary to inverse mapping the path obtained in the plane to 3D surface. The MABF algorithm has established the correspondence between the mesh in 3D and 2D, and it still needs to establish the correspondence of the points

in mesh between in the 2D and 3D. The area coordinate method is used to establish the correspondence of the points in mesh between in 3D and in 2D. This is because the area coordinates can ensure that the positional properties of the point in the triangle do not change during the inverse mapping process.

All pseudo-random path points in the plane are located in triangles in the plane mesh. Define $P(L_i, L_j, L_m)$, the path points in the triangle Δ_{ijm} , and convert Cartesian coordinates to area coordinates.

$$\begin{aligned}
 L_i &= \frac{S_{\Delta Pjm}}{S_{\Delta}} = \frac{[(x_j y_m - x_m y_j) + (y_j - y_m)x + (x_m - x_j)y]}{2\Delta} \\
 L_j &= \frac{S_{\Delta Pmi}}{S_{\Delta}} = \frac{[(x_m y_i - x_i y_m) + (y_m - y_i)x + (x_i - x_m)y]}{2\Delta} \\
 L_m &= \frac{S_{\Delta Pij}}{S_{\Delta}} = \frac{[(x_i y_j - x_j y_i) + (y_i - y_j)x + (x_j - x_i)y]}{2\Delta}
 \end{aligned}
 \tag{6}$$

Fig. 5 a The bicycle seat model. **b** The pseudo-random path in plane



where

$$S_{\Delta} = \frac{1}{2} \begin{bmatrix} 1 & x_m & y_m \\ 1 & x_i & y_i \\ 1 & x_j & y_j \end{bmatrix} = \frac{1}{2} [(x_i y_j - x_j y_i) + (y_i - y_j)x_m + (x_j - x_i)y_m] \tag{7}$$

After obtaining the area coordinates of point $P(x, y, z)$ in $\Delta ij m$ in 2D space, the corresponding triangle ΔIJM in 3D space is converted into Cartesian coordinates to obtain the corresponding point $P'(x', y', z')$ in 3D space.

$$\begin{bmatrix} x' \\ y' \\ z' \end{bmatrix} = \begin{bmatrix} x_i & x_j & x_m \\ y_i & y_j & y_m \\ z_i & z_j & z_m \end{bmatrix} \begin{bmatrix} L_i \\ L_j \\ L_m \end{bmatrix} \tag{8}$$

$$\begin{bmatrix} 1 & 1 & 1 \\ x_i & x_j & x_m \\ y_i & y_j & y_m \end{bmatrix} \begin{bmatrix} L_i \\ L_j \\ L_m \end{bmatrix} = \begin{bmatrix} 1 \\ x \\ y \end{bmatrix} \tag{9}$$

Arrange the path points after the inverse mapping in the order of the path points in the plane. By inverse mapping, the pseudo-random path planned in the plane is transferred to the 3D free-form surface, and the result is shown in Fig. 6.

4.2 Path smoothing based on NURBS interpolation

The pseudo-random path has a high degree of directional randomness. The spindle will start, stop, and change direction frequently during machining, resulting in fluctuating feed rates and low stability, which shocks the spindle and its accessories. The pseudo-random path is smoothed by using non-uniform rational B-splines (NURBS) curve interpolation, and the path is smoothed while ensuring that the path passes through all the dwell points. NURBS is a standard mathematical model representing curves and surfaces in computer modeling. The NURBS curves are defined by three parameters: control point, weight factor, and node vector. The NURBS curves are defined as Eq. 10.

$$P(u) = \frac{\sum_{l=0}^n \omega_l d_l N_{l,K}(u)}{\sum_{l=0}^n \omega_l N_{l,K}(u)} \tag{10}$$

where

$$\begin{cases} N_{l,0} = \begin{cases} 1 & \dots \dots \dots u \in [u_l, u_{l+1}] \\ 0 & \dots \dots \dots \text{otherwise} \end{cases} \\ N_{l,K}(u) = \frac{u - u_l}{u_{l+K+1} - u} N_{l,K-1}(u) + \frac{u_{l+K} - u}{u_{l+K} - u_{l+1}} N_{l+1,K-1}(u) \end{cases} \tag{11}$$

Gordon et al. defined the order of the NURBS curves p as 3, then the order K is $(p+1) = 4$. The node vector is shown in Eq. 12 [17].

$$U = [u_0, \dots, u_m] = \left[0, 0, 0, 0, \frac{l_1}{\sum_{l=1}^{m-p-1} l_l}, \frac{l_1 + l_2}{\sum_{l=1}^{m-p-1} l_l}, \dots, \frac{\sum_{l=1}^{n-K-1} l_l}{\sum_{l=1}^{m-p-1} l_l}, 1, 1, 1, 1 \right] \tag{12}$$

To improve the interpolation efficiency, Ji et al. represented the NURBS curve in matrix form as in Eq. 13 [18].

$$P(u) = \frac{\sum_{l=0}^n \omega_l d_l N_{l,3}(u)}{\sum_{l=0}^n \omega_l N_{l,3}(u)} = \frac{a_3 u^3 + a_2 u^2 + a_1 u + a_0}{b_3 u^3 + b_2 u^2 + b_1 u + b_0} \tag{13}$$

where $a_0, a_1, a_2,$ and a_3 are the coefficients of node parameters in the numerator, and $b_0, b_1, b_2,$ and b_3 are the coefficients of node parameters in the denominator. The Adams-Bashforth and Adams-Moulton methods were used to perform the parameter densification process, and the interpolation method uses equal-periodic interpolation. As an example, Fig. 7 shows a NURBS curve (blue curve) controlled by pseudo-random path points (little red dots) in three-dimensional space in Section 4.1.

Fig. 6 Pseudo-random path planning result on a 3D bicycle seat

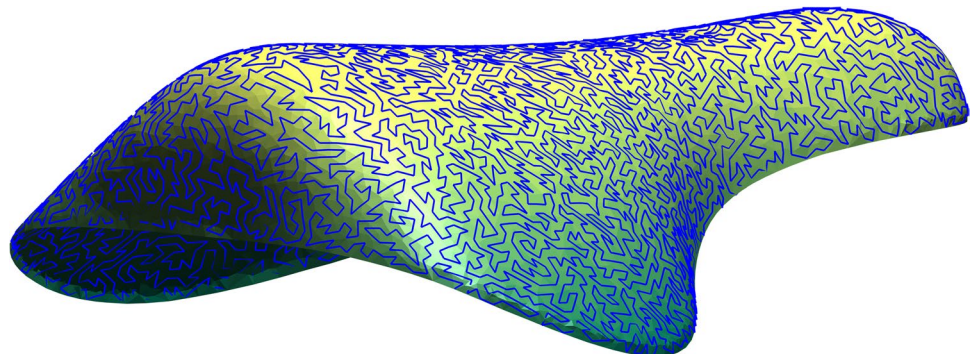
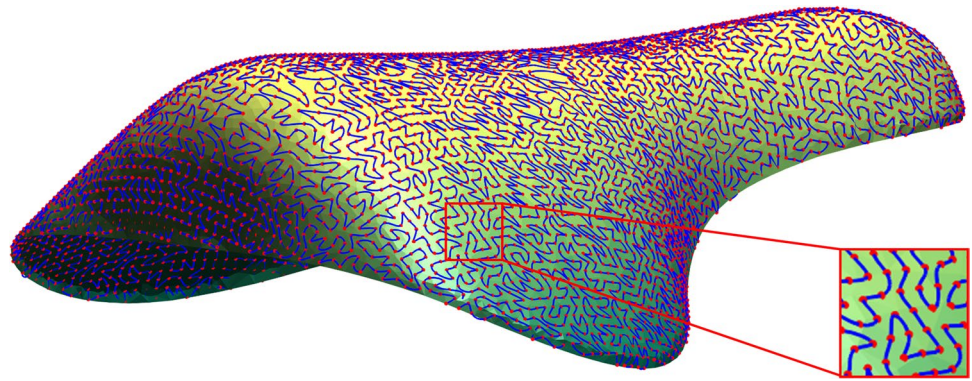


Fig. 7 Pseudo-random path on a bicycle seat after NURBS smoothing



5 Discussion and application

Previous pseudo-random path planning methods had a limitation of only being used in the plane range. However, the proposed method for planning pseudo-random path on 3D complex free-form surfaces has broken through this limitation. This extension of pseudo-random paths to 3D space allows for wider applications. Dunn et al. proposed a unicursal random tool path that never intersected for CNC machining, as shown in Fig. 8a [19]. The method only introduces directional randomness in a specific area, failing to provide the global randomness for the path, requiring improved randomness. Zhang et al. proposed a pseudo-random tool path based on the perfect maze to reduce the HSF errors left by the small polishing tool, as shown in Fig. 8b [20]. This path has low directional randomness, as it only has two directions of randomness. Furthermore, part of the path lies beyond the polishing area boundary, increasing the risk of collision between the polishing tool and workpiece fixture. Moreover, the pseudo-random path based on perfect maze can only accommodate two boundaries in the same path direction. This is because the path planning process considers the first and second boundaries that appear successively as the marks of entering and

exceeding the polished region. As a result, the path planning method based on perfect maze becomes less adaptable to the boundary of complex polished regions. Therefore, it becomes challenging to achieve path planning for the regions with complex boundaries. The random fractal-like path proposed by Dong et al. to suppress surface ripples is also an in-plane path planning method [4]. Although this method has a high degree of directional randomness and boundary adaptability, the path after smoothing has deviated from the dwell points, as shown in Fig. 8c. This will cause a significant deviation in the material removed during deterministic polishing and affect the surface accuracy after polishing.

To evaluate the performance of the pseudo-random path planning method based on the space MABF mapping, the machining path planning of a hemispherical surface (radius: 30 mm, triangular mesh number: 100220) was carried out by this method. The control group uses a pseudo-random path planning method based on the projection method, which can also be used for surface path planning. In this case, the path points were set at a lateral and longitudinal distance of 0.5 mm. Table 2 shows the path data obtained by the two methods, and Fig. 9 shows the distribution of the path on the hemisphere.

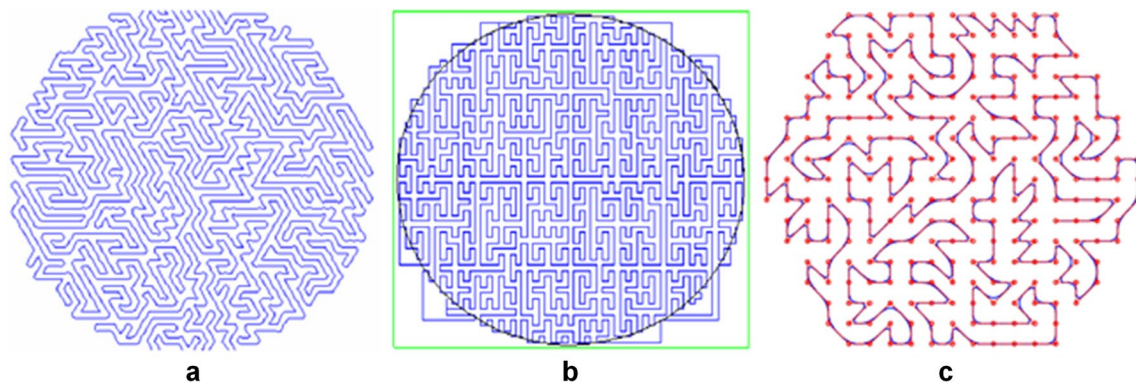


Fig. 8 a Unicursal random tool-path [19]. b Pseudo-random tool path based on the perfect maze [20]. c Random fractal-like path [4]

Table 2 Data obtained from trajectory simulation

Method	Average path step	Number of dwell points	Maximum step
Projection method	0.85325 mm	2836	3.6189 mm
Space MABF mapping method	0.5283 mm	7017	0.8592 mm

Each path point has eight moveable directions, so a machining path step between 0.5 and 0.7071 mm is considered normal. The average step of the path obtained by the projection method has exceeded the normal range, and its maximum step greatly surpassing normal value. The excessive path step will lead to a large chord error due to overcutting or undercutting, which will seriously affect the profile accuracy of workpiece. In Fig. 9a, the path obtained by the projection method shows an obvious overcutting phenomenon at the edge of the hemispherical surface. The average step obtained by the MABF method is still within the normal range, but the maximum step is slightly larger than the normal range. To address the issue, a step reduction factor of slightly less than 1 can be introduced when setting the initial step. In summary, the path planning method based on space MABF mapping outperforms the projection method in terms of path uniformity, the number of dwell points, and the path step.

The proposed mesh surface pseudo-random path planning method based on the space MABF mapping can adapt to the complex free-form surface. The machining path planned using this method has high direction randomness, is not restricted by the shape of the free-form surface boundary, and has high adaptability to the surface boundary. The proposed method is adaptable to surface curvature changes and can plan pseudo-random paths with a high fitting degree and good uniformity on complex surfaces. In addition, NURBS smoothing is applied to the planned pseudo-random path, and the smoothed path still passes through all the set dwell points precisely, which ensures the accuracy of the removal amount of each dwell point. The comparison of different algorithms is shown in Table 3. In the table, the total number of directional degrees of freedom is 8, and path accuracy refers to whether the planned path accurately passes through the preset dwell points.

Some cases are used to verify the effectiveness of the proposed pseudo-random path planning method based on space MABF mapping. Figure 10 shows the planning results. Based on the results obtained, the proposed path planning method offers several advantages, such as strong adaptability to surface boundaries, good path smoothness, path uniformity, and high proximity of path to the surface. It can efficiently and effectively generate a pseudo-random machining path for a complex free-form surface, ensuring high-precision and high-quality machining in subsequent processes.

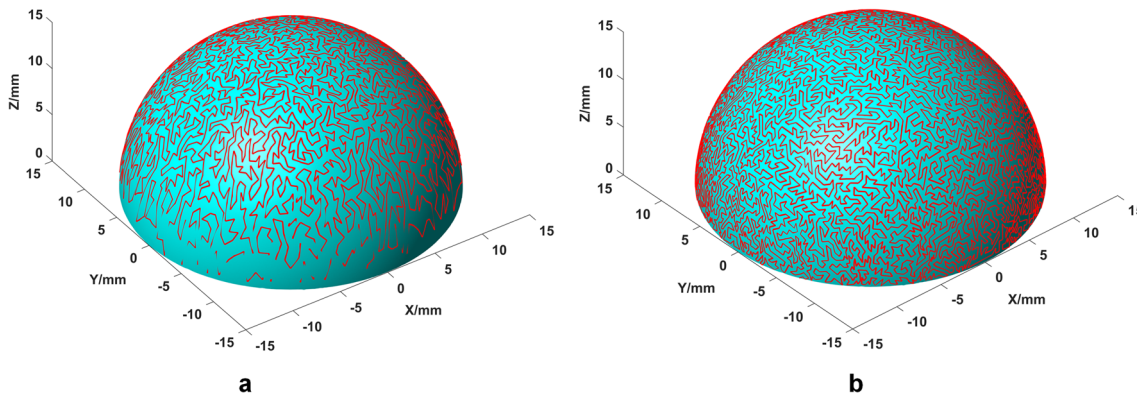


Fig. 9 a Path obtained by projection method. b Path obtained by the pseudo-random path planning method based on space MABF mapping

Table 3 Performance comparison of some pseudo-random paths

Path type	Directional degree of freedom	Boundary adaptability	Surface adaptability	Path uniformity	Path accuracy
Unicursal random tool-path	6/8	Y	N	Y	N
Pseudo-random path based on perfect maze	4/8	N	N	Y	Y
Random fractal-like path	8/8	Y	N	Y	N
Pseudo-random path based on the projection method	8/8	Y	Y	N	Y
Pseudo-random path based on space MABF mapping	8/8	Y	Y	Y	Y

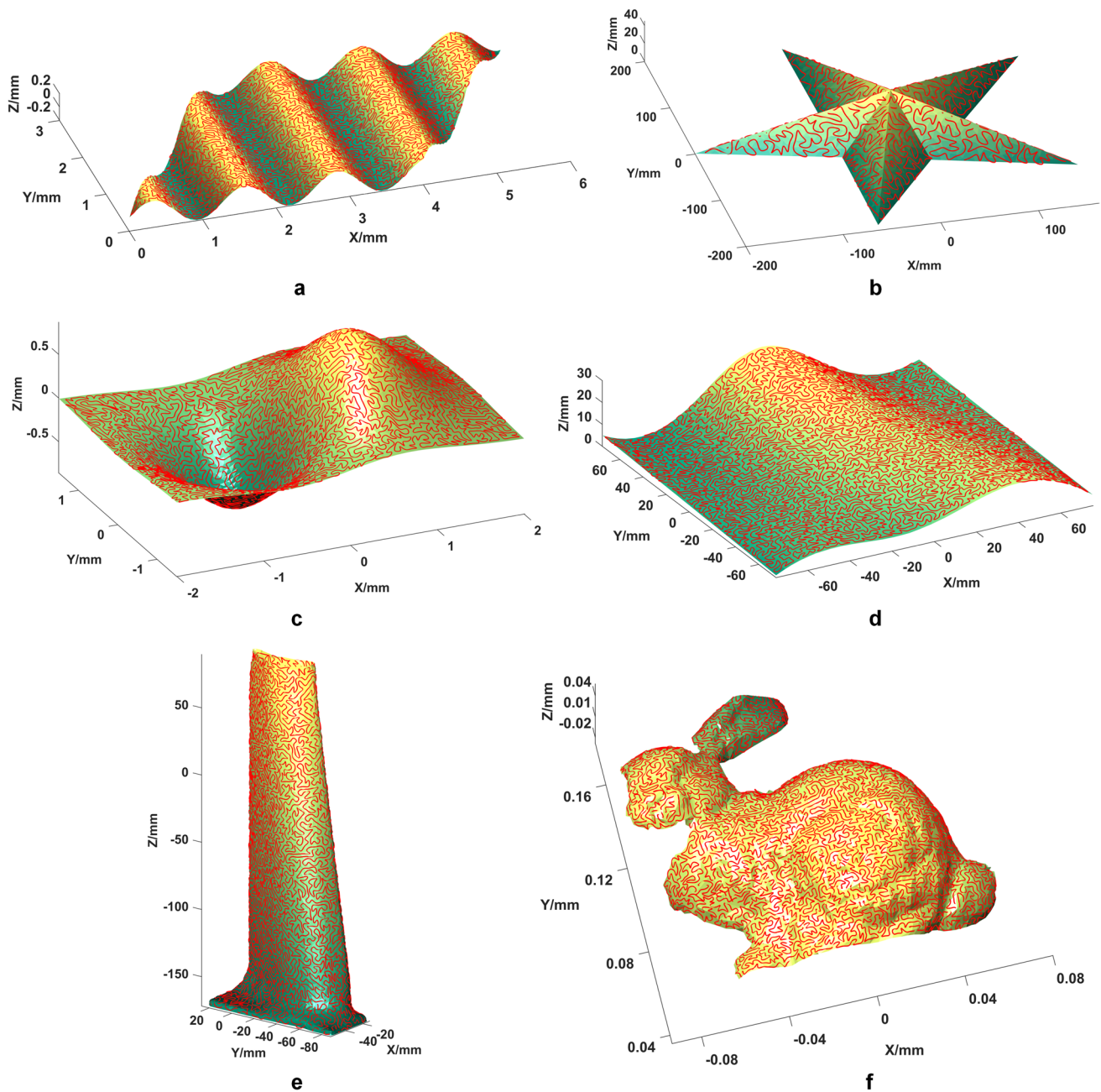


Fig. 10 Planning results for different cases. **a** Sinusoidal surface. **b** Pentagram surface. **c** Concave-convex surface. **d** Bicubic B-spline surface. **e** Airfoil surface. **f** Rabbit surface model

6 Experiment

To further verify the effectiveness of the pseudo-random path planning based on space MABF mapping method to suppress the M-HSF errors in the polishing process, we conducted comparative experiments using four different machining paths. The polishing tool used in the experiments was a polishing sponge, and an alumina-based polishing liquid was used as the polishing medium. The

polishing liquid was sprayed uniformly onto the surface of the workpiece using a peristaltic pump and an ultrasonic nozzle. The machining experiment uses a three-axis machine developed by the lab, shown in Fig. 11. The spindle motor is mounted on the Z-axis slide board, and the polishing liquid is continuously added during the polishing process using an ultrasonic nozzle. After surface meshing, planar parameterization, pseudo-random path planning, inverse mapping, and path smoothing, the pseudo-random

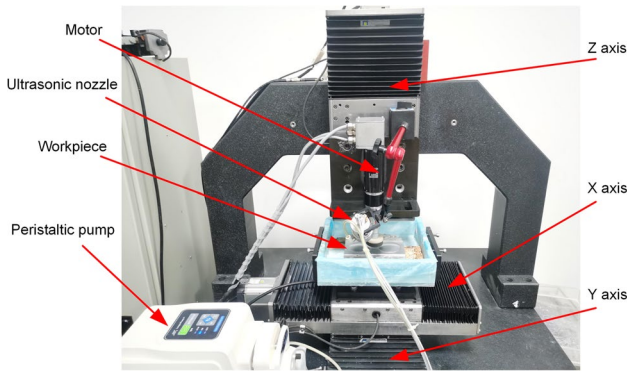


Fig. 11 Three-axis machining equipment

machining path is in the form of spatial coordinates containing X , Y , and Z parameters in order of the path. The 3-axis machine reads the machining path data file. After starting the machine, the machine will control the movement of the three motion spindles based on path data. The shape of the workpiece is the spherical crown. Form Taly-surf PGI 1240 surface profilometer was used to measure the surface of the workpiece before processing. The polishing tool uses a sponge head, and the abrasive grains in the polishing liquid are alumina oxide. The polishing tool rotates at a speed of 230 rpm, and all machining parameters were kept constant during the experiment.

The polishing experiments used different path types such as pseudo-random path based on space MABF mapping, raster path, spiral path, and rectangular path. The

dwell point spacing of machining paths was uniformly set to 0.5 mm. Each workpiece is polished twice for a total of 6 h. The polished workpieces are shown in Fig. 12, and the surface data was measured again. The collected measurements were processed, and the PSD curves of the surface using two polishing paths were depicted, as shown in Fig. 13. Table 4 displays the average PSD values for various paths in the 10^3 – 10^5 m^{-1} spatial frequency range before and after polishing. The suppression rates of several periodic paths are similar after polishing, and only the pseudo-random path obtains a significantly higher suppression rate. The experimental results show that using pseudo-random paths in the polishing process is more effective than using periodic paths in suppressing errors in the M-HSF range.

7 Conclusion

A mesh surface pseudo-random path planning method based on space MABF mapping is proposed to suppress the M-HSF errors generated in the polishing process of precision free-form surface optical components. The proposed method involves several stages: planar parameterization of spatial mesh surface based on the MABF algorithm, pseudo-random path planning in the plane, inverse mapping of the path to spatial surface, and smoothing of the path based on NURBS curves. The polishing path will be generated from the center of the mesh surface. Once the step of the dwell point is determined, the path-planning process can be performed heuristically without human intervention.

Fig. 12 The surface of the workpieces after polishing

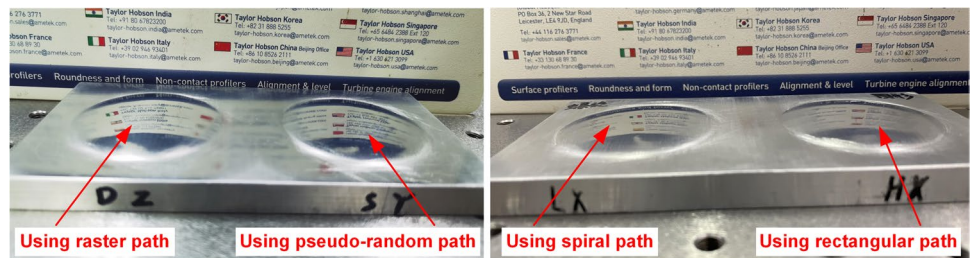


Fig. 13 a PSD curves of workpiece surface before polishing. b PSD curves of workpiece surface after polishing

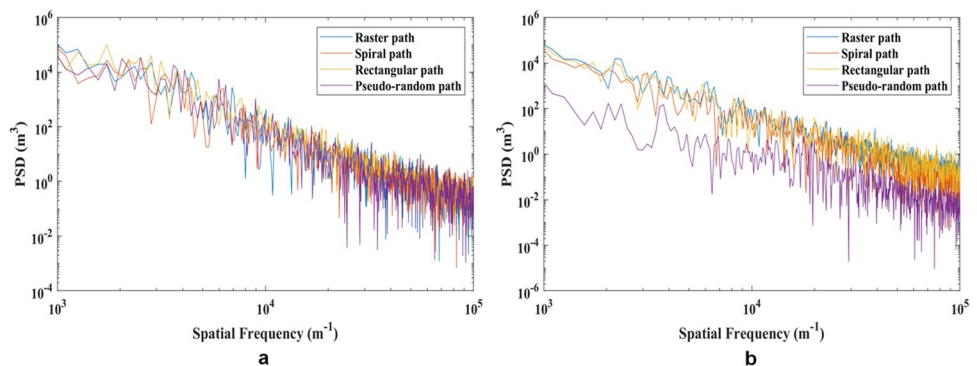


Table 4 The average PSD of the workpiece surfaces in the spatial frequency range of 10^3 – 10^5 m^{-1} before and after polishing

Path type	Average PSD before polishing	Average PSD after polishing	Suppression ratio
Raster path	0.596	0.393	34.06%
Spiral path	0.527	0.280	46.86%
Rectangular path	0.816	0.383	53.06%
Pseudo-random path based on space MABF mapping	0.566	0.019	96.64%

The MABF algorithm improves computational efficiency and error control compared to ABF. The MABF algorithm effectively improves planar parameterization accuracy. The advantages become more pronounced with an increasing number of meshes. The path smoothing method based on the NURBS curve interpolation not only smooths the path but also ensures that the path passes through each dwell point, which minimizes the impact of the path smoothing on the removal accuracy of each dwell point. Smooth pseudo-random paths with a high degree of directional randomness can suppress the generation of M-HSF errors in the polishing process, which is also verified in the polishing comparison experiments with periodic paths.

The proposed path planning method can effectively be used on complex mesh surfaces. Simulation results from various complex cases prove the versatility and robustness of the method. The proposed method can quickly obtain uniformly distributed pseudo-random paths on free-form surfaces. The error suppression strategy in this study is to increase the randomness of the machining path, which is not constrained by the shape of the workpiece. Using pseudo-randomized machining paths results in better error suppression capacity than periodic paths for any surface shape under the same process parameters. In addition, the pseudo-random path generation method proposed in this study can be combined with traditional polishing, magnetorheological polishing, jet polishing, milling, and even single-point diamond turning to improve the surface quality of machined parts. The idea of this study is to transform and process path coordinates, allowing the proposed path generation method to be utilized based on demand. However, the proposed path planning method needs to consume much time when there are a large number of dwell points. In the future, more efforts will be made to improve the efficiency of path planning further.

Supplementary Information The online version contains supplementary material available at <https://doi.org/10.1007/s00170-023-12801-3>.

Author contribution All authors contributed to the study's conception and design. Wei Wang wrote the first and final draft of the manuscript. Ruxin Gong undertook the main work of the experimental part, and Xiaoya Li was responsible for the simulation part. Shijun Ji and Ji Zhao reviewed the manuscript critically and all authors commented on previous versions. All authors read and approved the final manuscript.

Funding This work is supported by Science Center for Gas Turbine Project (P2022-A-IV-002-003), Key R&D Projects of the Ministry of Science and Technology of China (Grant No. 2018YFB1107600), National Natural Science Foundation of China (Grant No. 51775237), and Key R&D Projects of Jilin province of China (Grant Nos. 20200401121GX, 20230401099YY, and 20200401144GX).

Declarations

Competing interests The authors declare no competing interests.

References

- Tuell M, Burge J, Anderson B (2002) Aspheric optics: smoothing the ripples with semi-flexible tools. *Opt Eng* 15:1473–1474. <https://doi.org/10.1117/1.1481898>
- Achilles K, Uhlendorf K, Ochse D (2015) Tolerancing the impact of mid-spatial frequency surface errors of lenses on distortion and image homogeneity. *Opt Syst Des* 2015: Opt Des Eng VI 9626. <https://doi.org/10.1117/12.2191261>
- Liang FS, Kang CW, Fang FZ (2020) A smooth tool path planning method on NURBS surface based on the shortest boundary geodesic map. *J Manuf Process* 58:646–658. <https://doi.org/10.1016/j.jmapro.2020.08.047>
- Dong ZC, Nai WZ (2018) Surface ripple suppression in subaperture polishing with fragment-type tool paths. *Applied Optics* 57:5523–5532. <https://doi.org/10.1364/Ao.57.005523>
- Nie XQ, Li SY, Dai YF, Song C (2013) A new polishing process for large-aperture and high-precision aspheric surface. *Pacific Rim Laser Damage 2013: Optical Materials for High Power Lasers* 8786. <https://doi.org/10.1117/12.2020992>
- Feng YP, Cheng HB, Hu M, Zhang SH, Miao YL (2022) Influence and suppression of periodic contour error of tool path and velocity deviations on surface error. *Appl Opt* 61:1369–1380. <https://doi.org/10.1364/Ao.446907>
- Wan KP, Wan SL, Jiang C, Wei CY, Shao JD (2022) Sparse bi-step raster path for suppressing the mid-spatial-frequency error by fluid jet polishing. *Opt Exp* 30:6603–6616. <https://doi.org/10.1364/Oe.453122>
- Hu H, Song C, Xie XH (2016) Combined fabrication technique for high-precision aspheric optical windows. *Adv Opt Mech Technol Telescopes Instrument II* 9912. <https://doi.org/10.1117/12.223220>
- Hoyo JD, Choi H, Burge JH, Kim GH, Kim DW (2017) Experimental power spectral density analysis for mid- to high-spatial frequency surface error control. *Appl Opt* 56:5258–5267. <https://doi.org/10.1364/Ao.56.005258>
- Lin XH, Zhang JB, Tang HH, Du XY, Guo YB (2017) Analysis of surface errors and subsurface damage in flexible grinding of

- optical fused silica. *Int J Adv Manuf Tech* 88:643–649. <https://doi.org/10.1007/s00170-016-8766-2>
11. Takizawa K, Beaucamp A (2017) Comparison of tool feed influence in CNC polishing between a novel circular-random path and other pseudo-random paths. *Opt Exp* 25:22411–22424. <https://doi.org/10.1364/Oe.25.022411>
 12. Zha J, Zhang HC, Li YP, Chen YL (2020) Pseudo-random path generation algorithms and strategies for the surface quality improvement of optical aspherical components. *Materials* 13:1216. <https://doi.org/10.3390/ma13051216>
 13. Huang Z, Chen GK, Liu HT, Rao ZM, Wu JL (2022) Research on robot bonnet polishing silicon carbide optical element machining method based on improved traveling salesman problem pseudo-random polishing path planning. *Optical Engineering* 61:025102. <https://doi.org/10.1117/1.Oe.61.2.025102>
 14. Maloney C, Lormeau JP, Dumas P (2016) Improving low, mid and high-spatial frequency errors on advanced aspherical and freeform optics with MRF. *Proc SPIE* 10009. <https://doi.org/10.1117/12.2236034>
 15. Dai YF, Shi F, Peng XQ, Li SY (2009) Restraint of mid-spatial frequency error in magneto-rheological finishing (MRF) process by maximum entropy method. *Sci China Ser E* 52:3092–3097. <https://doi.org/10.1007/s11431-009-0316-9>
 16. Beaucamp A, Takizawa K, Han YJ, Zhu WL (2021) Reduction of mid-spatial frequency errors on aspheric and freeform optics by circular-random path polishing. *Optics Express* 29:29802–29812. <https://doi.org/10.1364/Oe.435945>
 17. Gordon WJ, Riesenfeld RF (1974) B-spline curves and surfaces. *Comput Aided Geometr Des* 95-126. <https://doi.org/10.1016/B978-0-12-079050-0.50011-4>
 18. Ji SJ, Lei LG, Zhao J, Lu XQ, Gao H (2021) An adaptive real-time NURBS curve interpolation for 4-axis polishing machine tool. *Robot Cim-Int Manuf* 67:102025. <https://doi.org/10.1016/j.rcim.2020.102025>
 19. Dunn CR, Walker DD (2008) Pseudo-random tool paths for CNC sub-aperture polishing and other applications. *Opt Expr* 16:18942–18949. <https://doi.org/10.1364/Oe.16.018942>
 20. Zhang FH, Yu XB, Zhang Y (2011) Study on unicursal pseudo-random tool path for computer controlled polishing. *Adv Mater Res-Switz* 188:729–732. <https://doi.org/10.4028/www.scientific.net/AMR.188.729>

Publisher's Note Springer Nature remains neutral with regard to jurisdictional claims in published maps and institutional affiliations.

Springer Nature or its licensor (e.g. a society or other partner) holds exclusive rights to this article under a publishing agreement with the author(s) or other rightsholder(s); author self-archiving of the accepted manuscript version of this article is solely governed by the terms of such publishing agreement and applicable law.